Clays and Clay Minerals, Vol. 56, No. 5, 558–570, 2008.

SMECTITE CLAY SEQUESTRATION OF AFLATOXIN B_1: PARTICLE SIZE AND MORPHOLOGY

I. MULDER, A. L. BARRIENTOS VELAZQUEZ, M. G. TENORIO ARVIDE, G. N. WHITE, AND J. B. DIXON*

Soil and Crop Sciences Department, Texas A&M University, College Station, Texas 77843-2474, USA

Abstract—The properties that might influence the sequestration of aflatoxin B_1 (AfB_1) were examined. Laser-diffraction, particle-size analysis (LDPSA) indicated that the particle size of the smectite influences the amount of AfB_1 adsorbed. Effective adsorbent smectites disperse well under combined sodium hexametaphosphate solution and ultrasonic agitation. Particle size explained 66% of the variability for most of the samples investigated in an 'as-received' state. One effective adsorbent smectite was especially well aggregated and required additional physical dispersion, thus raising the correlation to 73%. Transmission electron microscope (TEM) images show typical smectites and reveal the very diverse morphology of smectites in bentonites. Thin, cloud-like smectite, in TEM images, related positively to AfB_1-adsorption capacity. Particles that often fold and are usually ~0.5 μm across seem to be optimal. The selection of criteria for evaluating these smectites provides a scientific basis for their selection to obtain reliable performance. Particle size is of particular importance as outlined below, and use of LDPSA makes it possible to perform the analysis efficiently and with precision.

Key Words—Adsorption, Animal Feed, Corn, Grain, Liver Cancer Prevention, Mycotoxin, Toxicology.

INTRODUCTION

Aflatoxins are secondary fungal metabolites that contaminate crops worldwide and are a risk to the economic performance of farmers and to the health of humans and animals who consume contaminated food or feed. To remediate the harmful effects of aflatoxin on farm animals, animal scientists have found an effective strategy: upon the addition of smectites to the animals' diets at levels as low as 5 g/kg, almost total protection from aflatoxicosis could be achieved. The adsorption of aflatoxin by smectite takes place inside the animal gastrointestinal tract (Phillips *et al.*, 2002).

The questions as to how and why aflatoxin B_1 molecules are adsorbed by the smectites are of pivotal importance in predicting good adsorbent material to protect animal health in the future and to assign quality labels to industrial aflatoxin-adsorbent products. Aflatoxin B_1 is largely a planar molecule with a molecular weight of 312 g/mole. The six O atoms contribute negativity to the molecule of Aflatoxin B_1 shown below.

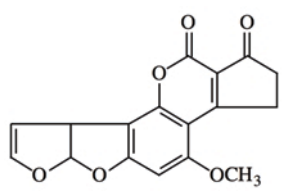

* E-mail address of corresponding author:
j-dixon@tamu.edu
DOI: 10.1346/CCMN.2008.0560509

In a previous study strong evidence was provided, by means of X-ray diffraction (XRD), that AfB_1 was adsorbed into the interlayer galleries of smectites (Kannewischer *et al.*, 2006). Desheng *et al.* (2005) came to the opposite conclusion, *i.e.* interlayer adsorption was not a factor, but their samples were tested at low AfB_1 saturation. Phillips *et al.* (2002), in an independent study, supported the hypothesis of interlayer adsorption of AfB_1.

Several theories for selective chemisorption of the AfB_1 by smectite can be found in the literature. Sarr *et al.* (1991) suggested, based on Fourier transform infrared spectroscopy (FTIR) findings, that the β-dicarbonyl of the AfB_1 molecule forms complexes with incompletely coordinated metal ions of a hydrated sodium calcium aluminosilicate (HSCAS). Phillips *et al.* (1995) agreed with this hypothesis for a binding mechanism in that the β-dicarbonyl system is an electron-rich system that should readily form complexes with unfilled d orbitals of transition metals. Computer modeling was used to show that AfB_1 may react at surfaces within the interlayer of HSCAS particles. Phillips (1999) suggested that AfB_1 may react as effectively on edge and basal surface sites of the HSCAS particles as on the interlayer sites. Phillips *et al.* (2002) proposed that a potential chemical binding reaction between the smectite surface and the AfB_1 molecule may be an electron donor/acceptor (EDA) mechanism.

In addition to the β-dicarbonyl group, Pavão *et al.* (1995) indicated that the furan rings of AfB_1 are likely to participate in thermodynamically favored epoxidation and hydroxylation reactions. These reactions are in agreement with Urbanek's (1997) suggestion that AfB_1

is bonding with DNA. Since those authors were working in a different adsorption system, the relevance of this type of reaction in the AfB_1-smectite system has yet to be determined.

Although the adsorption mechanisms of AfB_1 on a molecular scale are being discussed and modeled, the smectite properties that make them more effective or less effective adsorbents are not known (Dixon *et al.*, 2008). To find possible correlations of adsorptive capacity with clay properties, multivariate analysis was performed on a set of characteristics (Lee *et al.*, 2005). The results showed no clear correlations for any individual or combination of properties.

Many bentonites have been tested for adsorption of AfB_1. Correlations between exchangeable cations and cation exchange capacity (CEC) and the AfB_1 adsorption capacity were noted (*e.g.* Kannewischer, 2006). Recently, FTIR data have shown that the chemical composition of the smectites might be useful as an indicator to predict their qualities as AfB_1 adsorbents (Tenorio Arvide *et al.*, 2008). The presence of Mg and Fe in octahedral positions has been demonstrated to correlate with good adsorbent properties whereas predominantly Al in octahedral positions was a trait of the inefficient AfB_1-adsorbents.

In an effort to further explore properties that might influence the adsorption of AfB_1, a study of the effects of particle-size distribution on the adsorption of AfB_1; and a study using transmission electron microscopy (TEM) with selected area electron diffraction (SAED) to describe the clay morphology were undertaken.

MATERIALS

Samples 8TX (0.68 mol AfB_1/kg adsorption maximum), 1MS (0.53 mol AfB_1/kg), and 11ID (0.48 mol AfB_1/kg) were selected for a fractionation procedure because they had qualified previously as good AfB_1 adsorbents. Sample 5OK (0.13 mol AfB_1/kg) showed poor adsorptoin of AfB_1, as determined by adsorption isotherm analysis. The sample source is identified by the state abbreviation in the USA and by MX in Mexico.

A larger selection of untreated smectites from a set of 20 samples (Kannewischer *et al.*, 2006) was used for LDPSA and TEM (Table 1). In addition, a freeze-dried palygorskite from Florida and a relatively pure phlogopite- derived vermiculite from Llano, Texas, were used for comparative analysis. The vermiculite was machine-ground for 2 min with a mechanical grinder by Ångstrom, Inc., Chicago, Illinois.

Aflatoxin B_1 from *Aspergillus flavus* was purchased from Sigma Chemical Co. (St. Louis, Missouri); CAS No. 1162-65-8, Acetonitrile, Chromasolv® for HPLC, gradient grade was purchased from Sigma-Aldrich; CAS No. 75-05-8, Benzene, GR, CAS 71-56-1, and methanol, HPLC Grade, CAS 67-56-1, were from EM Sciences (Gibbstown, New Jersey).

METHODS

Fractionation and laser-diffraction particle-size analysis

Before the samples were fractionated they were pretreated to remove carbonates, organic matter (OM), and MnO_2. For each of the four samples, a 20 g subsample of the bulk material was used. Carbonates were removed by treating with 1 M NaOAc (pH 5) buffer solution while maintaining the temperature at 70ºC in a waterbath. To remove OM and MnO_2, the samples were treated with H_2O_2. To disperse the samples, they were saturated with Na using pH 10 Na_2CO_3 (Kunze and Dixon, 1986).

The sand fraction was obtained by sieving the samples through a 53 μm sieve. The silt (50−2 μm) and clay fractions were seperated gravimetrically *via* centrifugation according to Stokes' law (White and Dixon, 2003). Silt and coarse- (2−0.2 μm) and fine- (<0.2 μm) clay fractions were oven dried from suspension in water at 105ºC.

In addition to the fractionation procedures, bulk samples were analyzed for particle-size distribution using a laser-diffraction particle-size analyzer (LS230, Beckman Coulter). This instrument uses laser-diffraction technology and multi-wavelength light scattering to determine particle-size distribution in a single analysis employing binocular optics. One per cent clay samples were suspended by shaking overnight in water or sodium hexametaphosphate solution prior to laser-diffraction analysis. An ultrasonic probe was used for further physical dispersion in Na-hexametaphosphate solution before laser-diffraction analysis (Vibra-cell by Sonics with settings: amplitude 50, time 1 min, and pulse rate 4 s).

X-ray diffraction (XRD)

Slides with oriented particles were prepared for XRD analysis of the silt, coarse-clay, and fine-clay fractions by drying a sample from suspension in water on VICOR® glass slides. The sand fractions were X-rayed on sample holders with quartz plate support. The XRD patterns were obtained using a Philips X-ray

Table 1. Adsorption properties of bulk clays and of oven-dried coarse-clay (CC) and fine-clay (FC) fractions.

Sample	Q_{max} (mol/kg)	Langmuir R^2	Linear R^2
8TX FC	0.24	0.810	0.894
8TX CC	0.36	0.868	0.902
8TX bulk	0.68	0.898	0.776
1MS FC	0.27	0.753	0.981
1MS CC	0.34	0.923	0.909
1MS bulk	0.53	0.943	0.705
11ID FC	0.23	0.674	0.947
11ID CC	0.24	0.580	0.757
11ID bulk	0.48	0.916	0.498

diffractometer (Philips Electronic Instruments, Norelco, no. 12215/0, Mount Vernon, New York) with CuKα radiation, a graphite monochromator, and a theta-compensation slit. Each pattern was measured in 0.05º2θ intervals from 2 to 64º2θ to observe the first and higher-order smectite peaks and possibly other mineral phases (White and Dixon, 2003).

Isothermal adsorption procedure

Smectite (0.1 mg) was added to 5 mL of AfB_1 solutions with concentrations of 0.0, 0.4, 1.6, 3.2, 4.8, 6.4, and 8.0 mg/L. The amount of AfB_1 adsorbed was determined, after 24 h of shaking, using a UV/visible spectrophotometer. Data were fitted to the Langmuir equation. The method was described in detail by Kannewischer *et al.* (2006).

Transmission electron microscopy

Eight bulk smectites, 8TX, 1MS, 11ID, 17TX, 6WY, 7AZ, 5OK, and 16MX, and the coarse- and fine-clay fractions of samples 1MS, 8TX, 11ID, and 5OK were chosen for study. Suspensions of each smectite sample were prepared using ~1 g of untreated smectite sample in 5 mL of distilled water in glass test tubes. They were dispersed for 2 min in an ultrasonic bath, after which they were allowed to settle for 30 min. An aliquot of the clay suspension was transferred to a small glass jar and diluted with distilled water until it was almost transparent. To mount the clay on a carbon-coated Formvar® copper grid, one drop was pipetted onto the grid and dried under a heat lamp. The grids were examined in a JEOL JEM-2010 electron microscope operated at an acceleration voltage of 200 keV. Electron images were recorded at calibrated magnifications (between 14,710× and 205,062×) on Kodak Electron Microscopy Film 4489. For digitization of the electron micrographs, films were scanned at 42.3 μm increments corresponding to pixel sizes between 2.88 and 0.21 nm at the specimen level (*cf.* Holzenburg *et al.*, 1996). For each sample, pictures were taken from five locations on different quadrants of the grid at high magnification. Additionally, one overview image was taken at 14,710× magnification for each sample. Exceptions were samples of fractions where pictures of four to five locations were taken. Selected area electron diffraction data were obtained whenever possible.

RESULTS

Characterization of as-received clays

The 14 bentonite clay samples from the USA and Mexico have a ten-fold range of AfB_1 adsorption (Table 2). They are alkaline except for sample 17TX which is very acid. The major exchange cation is Ca in most of the samples except for 6WY and LC1 where Na is the major exchange cation. The XRD data are consistent with the abundant exchange of Ca, the smallest spacing being in 6WY, with abundant exchangeable Na. All samples collapsed on K-saturation and heating, indicating free interlayer space for adsorption. The only exception is sample 17TX, which apparently has a little interlayer hydroxy-Al as suggested by its acid pH. Some salts may contribute to the extractable bases. The CEC values were determined at a controlled pH to measure the smectite clay present because it is the major clay mineral present and has a large CEC value. The CEC values do not address the octahedral ion concentration in the smectite.

Analysis of fractionations

The distribution of sample fractions prepared by a sodium carbonate dispersion procedure after removal of flocculating agents (salts, organic matter, *etc*.) is given in Table 3. On average, more than 20% of the starting material was lost during the fractionation process, ranging from 16% for sample 5OK to 31% loss of starting material for 11ID. Except for sample 1MS, all samples consisted of 60% or more coarse and fine clay based on normalized values. Sample 1MS had 40% silt, yet it was a good adsorbent of AfB_1 as discussed below.

In the XRD patterns, the major diversity in mineralogy existed in the sand fraction of the samples as expected (Figure 1). Minerals in the sand fraction of all samples were mostly quartz and feldspars (plagioclase, anorthite). Sample 8TX contained dolomite and probably quartz. The quartz peak indicated for 8TX in Figure 1 shares the same *d* spacing (0.334 nm) as dolomite and seemed to lack the intensity typical of quartz. In the sand fractions, no smectite peaks were present except for weak ones in sample 8TX.

Silt XRD patterns showed smectite and quartz peaks. Sample 11ID had a smectite peak of the same relative height as the quartz peak, and for 1MS and 5OK samples, quartz was the strongest XRD peak.

All coarse- and fine-clay fractions (CC, FC) contained almost exclusively first- and fourth-order smectite peaks. Second- and third-order peaks of smectites were only weakly expressed. In the clay fractions no other mineral peaks were visible (Figure 1).

Adsorption data for coarse clay fractions are presented in Figure 2. Adsorption values were consistently larger for the bulk material which had not been oven dried. The dispersion and subsequent oven drying apparently created persistent aggregates that reduced their adsorption of the mycotoxin molecules (Table 1). The coarse-clay fractions adsorbed more AfB_1 than the fine clays. The adsorption observed for sample 5OK was very small, *i.e.* <0.05 mol/kg for the CC, its strongest adsorbing fraction (Figure 2). Sample 5OK CC was an exception with its low adsorption, and the Langmuir equation was not applicable.

Palygorskite and vermiculite were also analyzed and had almost zero adsorption capacity for AfB_1.

Table 2. Some properties of the unfractionated smectite samples.

Sample	Analysis	— Langmuir equation — Maximum adsorption capacity Q_{max} (mol/kg)	R^2	pH	—— NH_4OAc-extractable bases —— Ca	Mg	Na	K	CEC in NaOAc	——— *d* spacing (XRD) ——— As received	K-saturated	K-saturated at 550ºC
					——— ($cmol_c/kg$) ———					——— (nm) ———		
8TX	L, T, F	0.68	0.98	7.1	54.6	21.8	8.3	1.0	84.1	1.39	1.13	0.99
1MS	L, T, F	0.53	0.95	8.3	94.1	9.4	0.4	1.5	85.8	1.38	1.15	1.02
T7	L	0.52	0.99	8.8	51.7	15.3	43.5	0.5	87.6	1.46	1.17	0.98
11ID	L, T, F	0.48	0.97	7.4	56.6	15.6	9.2	0.7	76.4	1.51	1.11	0.99
T4	L	0.40	0.92	8.5	92.1	12.9	0.6	1.5	99.9	1.36	1.25	0.98
14MS	L	0.40	0.93	7.7	97.9	13.8	0.5	1.9	84.3	1.47	1.14	1.01
17TX	L, T	0.38	0.98	4.7	36.8	17.4	10.7	1.0	78.4	1.47	1.29	1.02
3MS	L	0.32	0.97	8.6	90.6	9.8	0.4	1.5	94.3	1.49	1.14	1.06
6WY	T	0.29	0.95	9.6	15.5	4.5	83.6	1.1	83.3	1.26	1.12	0.97
2MS	L	0.28	0.94	8.7	93.3	9.2	0.4	1.7	85.4	1.49	1.16	1.02
7AZ	L, T	0.15	0.69	7.6	96.9	19.2	1.0	1.2	90.1	1.45	1.23	1.02
5OK	L, T, F	0.13	0.89	7.3	78.5	23.4	1.1	0.4	101.3	1.52	1.19	1.00
LC1	L	0.12	0.90	10.1	37.5	10.4	63.0	14.3	62.1	1.41	1.25	0.99
16MX	L, T	0.06	0.96	7.6	20.0	22.6	12.1	2.0	68.3	1.58	1.23	1.04

L: Laser diffraction particle-size analysis
T: Transmission electron microscopy
F: particle-size fractionation

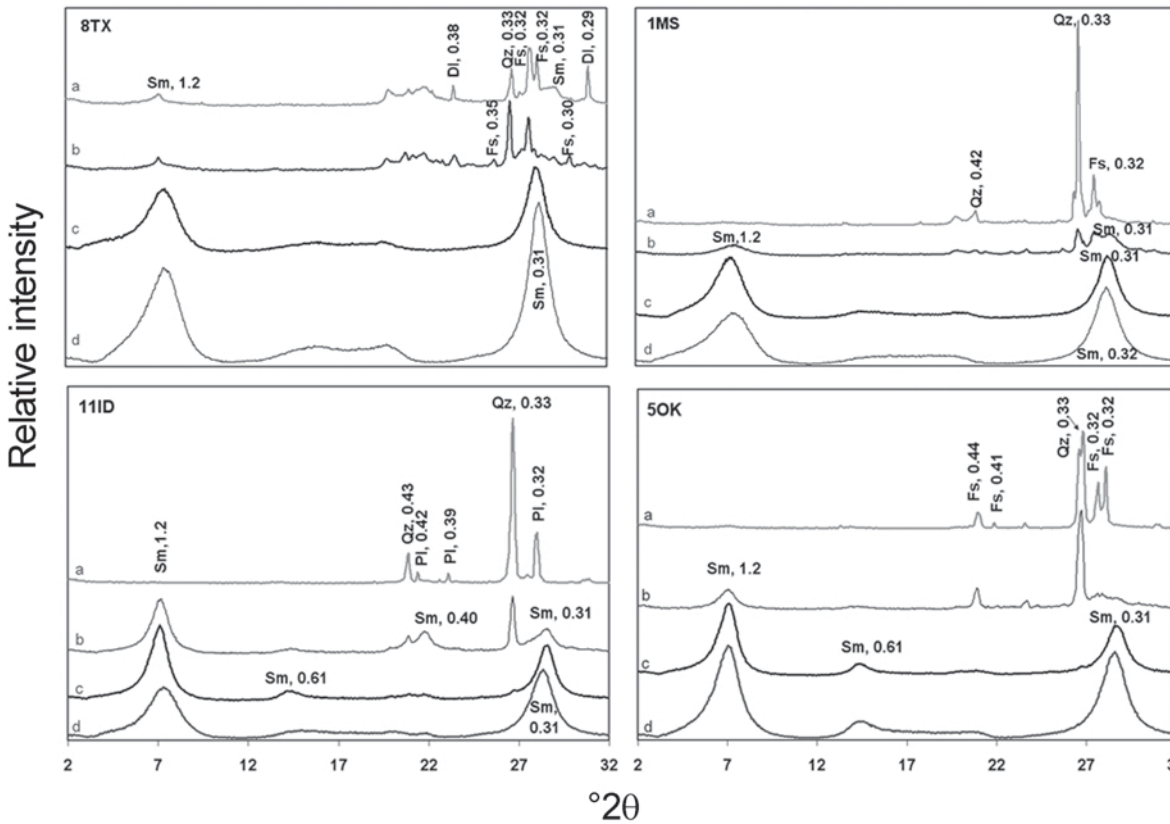

Figure 1. XRD patterns of sand, silt, coarse-clay, and fine-clay fractions of samples 8TX, 1MS, 11ID, and 5OK in the range 2–32°2θ. Sm = Smectite, Qz = Quartz, Fs = Feldspar, Dl = Dolomite, Gt = Goethite, Pl = Plagioclase. The *d* spacings are in nm. Goethite in 1MS causes the yellow color of that sample.

Transmission electron microscopy

Selected TEM and SAED patterns of clay fractions of the four fractionated samples are displayed in Figure 3. Overall, morphologies appear to be those of typical smectites for all samples, with many small thin particles in the viewing field that were often not very distinct from the surroundings. In the SAED patterns, diffuse rings were observed for all samples, which are caused by the turbostratic structure of smectites (Mering and Oberlin, 1971). This means that the layers of the smectites are disordered in the (a,b) plane with respect to the *a* and *b* crystallographic axes but not to the *c* axis. Depending on degree of stacking disorder, the particles of the samples observed had more or less diffuse rings, with a tendency for 1MS and 11ID to have sharper rings, and of 8TX and 5OK to have more diffuse rings.

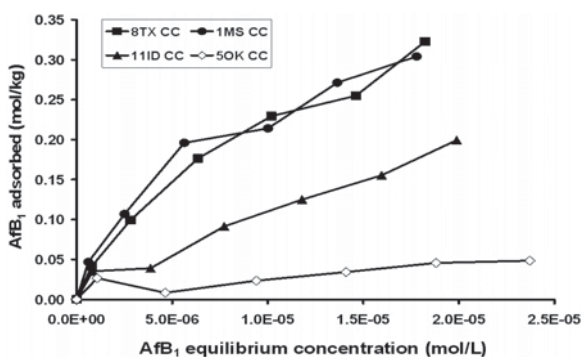

Figure 2. Aflatoxin adsorption by coarse-clay fractions *vs.* concentration of aflatoxin in water..

The electron micrographs for 8TX and 1MS in Figure 3 are characterized by overall complex shapes with complex curvature or cloud-like diffuse material. The curvature of particles is predominant in sample 8TX. The corresponding SAED pattern shows diffuse rings, and no sharp rings or spot pattern were observed.

The images of sample 1MS show mainly thin particles that were frequently folded. In the SAED pattern, sharp rings indicating higher order within the *a*–*b* crystal plane are shown, which were common for this sample. In addition to the crisp edges as shown here, the specimen also contained rather diffuse particles.

The micrographs of 11ID showed several different features. The SAED pattern of a thick particle (Figure 3e) shows a spot pattern, suggesting mica or illite. Diffuse (thin) edges in the material (Figure 3e,f) are mixed with more cloudy smectites (Fig. 3f). The SAED pattern of Figure 3f showed several rings, indicating smectite. Another location in the sample,

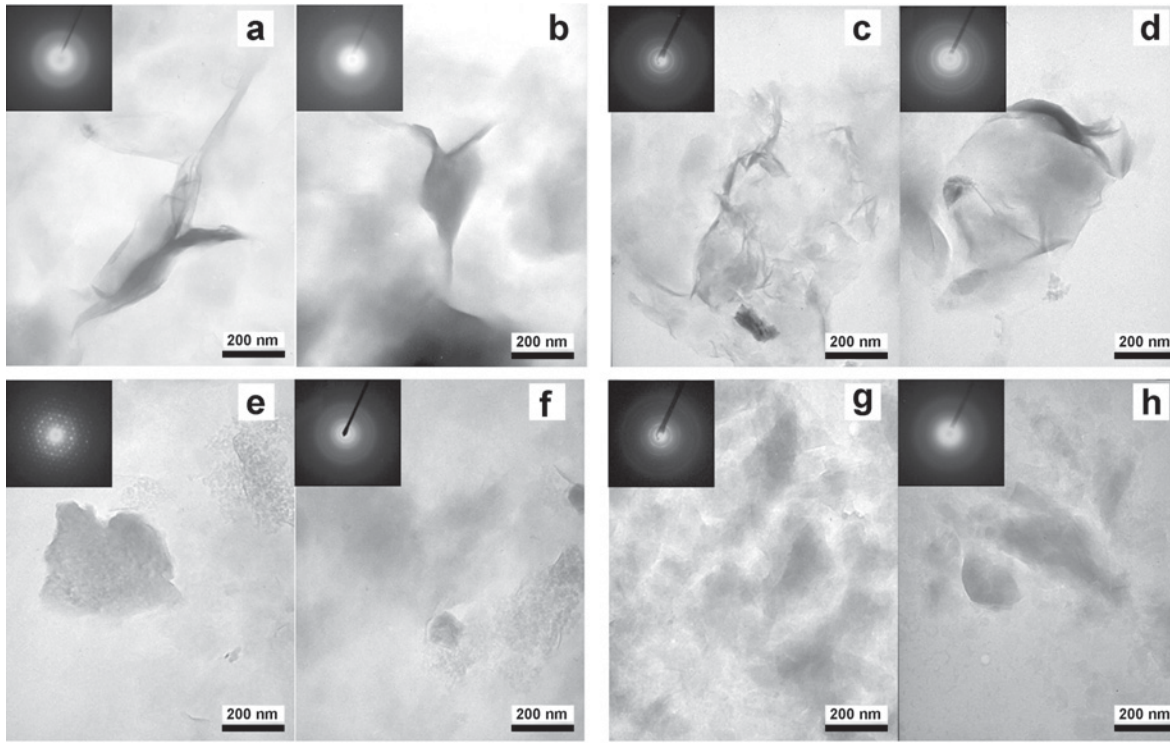

Figure 3. Electron micrographs of the clay fractions of samples 8TX (a,b), 1MS (c,d), 11ID (e,f), and 5OK (g,h).

not displayed here, showed sharper rings than typical for smectite, and may indicate the presence of more highly ordered phyllosilicate phases. In both images of 11ID, some rolled edges were observed. The mixture of materials indicates a natural origin of the sample.

The images of sample 5OK show typical smectite with small, thin particles (Figure 3g,h). Rounded edges and the absence of crisp detail may be a sign of weathering. The SAED pattern has weak diffuse rings suggesting poor crystallinity. The EDS data on this sample indicate that all four observed locations on the sample contain very little or no Fe as observed by EDS (data not shown). Also, the sample is white in color.

The micrographs in Figure 4 were chosen to show the diversity within the set of eight samples. Sample 8TX contains laths that have undergone beam damage. These laths are probably of gypsum and the disruptions, bubble-like protrusions in the lath to the left, probably indicate loss of structural water. Sample 1MS has thin, rolled edges, suggesting thin smectite. Sample 11ID has numerous small clusters of particles assumed to be smectite. Sample 17TX is a complex assembly of tightly rolled sheets in a cluster constituting a large linear bundle. Sample 6WY is a well rounded, large particle (300 nm $\times$ 400 nm) with layers visible near the edges suggesting weathering of thin edges. Sample 7AZ is more characteristic of smectite, thicker in the middle, and with very thin edges, irregular in shape with few dark lines suggesting folding of sheets. Sample 5OK is a large particle that seems to have retained the shape of a previous substrate, resembling a collection of glass fibers (possibly opaline silica). Sample 16MX resembles the morphology of vesicular glass that may have been altered to smectite.

All samples contained particles with rolled edges and folds typical of smectites and these features are displayed in the electron micrographs of samples 1MS, 11ID, 17TX, and 7AZ, respectively (Figure. 4). Micrographs of samples 6WY and 5OK (Figure 4) appear thicker than typical smectites. Sample 11ID (Figure 4) shows a cluster of globular material, another form in which smectites may occur (Grim and Güven, 1978). The globular smectites were encountered frequently throughout that sample. The micrograph of 8TX shows an example of the frequently occurring laths suggestive of gypsum (see also Figure 5). The micrographs for 16MX (Figure 4) show a complex morphology, which, hypothetically, could have evolved from the diatomaceous components in that specimen and it has lattice fringes suggestive of a layer silicate, calculated to be ~4 nm.

The SAED patterns mostly show weak, diffuse rings, indicative of smectite (Figure 4). Adsorbents 7AZ, 5OK, and 16MX exhibited more well defined particles with less cloudy (thin), dispersed smectites and particles which were larger overall. Sample 11ID, a good

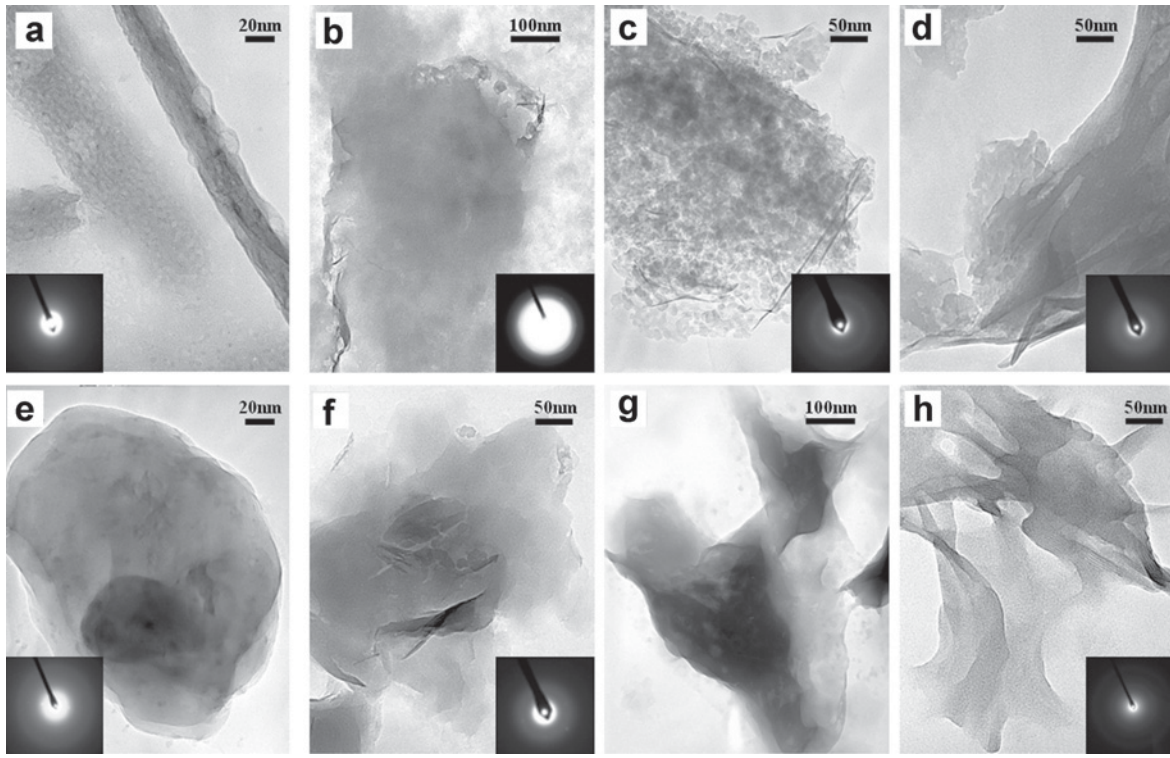

Figure 4. Electron micrographs of samples: 8TX (a), 1MS (b), 11ID (c), 17TX (d), 6WY (e), 7AZ (f), 5OK (g), and 16MX (h) at magnifications between 80,000 and 200,000 × with their SAED patterns.

adsorbent, appears, similar to the overview image, to have more cloudy and globular smectites as shown in Figure 3. A genetic relationship between samples 8TX and 17TX is suggested by the presence of laths, assumed to be gypsum identified elsewhere by XRD.

Figure 5 comprises micrographs at lower magnification. The differences between the morphologies of the most effective and least effective adsorbents suggest a relationship between particle size and the amount of AfB_1 adsorbed. The three best adsorbents, 8TX, 1MS, and 11ID, have particles with shades of gray and many fine particles are evident in samples 8TX and 1MS. Sample 11ID has few fine particles, yet it is one of the better adsorbents of the mycotoxin (Table 1). Sample 17TX has a diversity of particles: some gypsum laths, fine particles, and one large particle that is partially opaque on the edges, yet it has many fine particles too. The gypsum and the larger opaque particles probably account for its moderate mycotoxin adsorption. Two of the poorest adsorbents, 5OK and 16MX, have increasingly evident opaque (black) particles (Figure 5) and few fine particles, as shown by the mode exceeding 5 μm. Samples 5OK and 7AZ also have cation exchange values of 101 and 90 cmol/kg, respectively, suggesting an excessively high charge for optimum adsorption of the mycotoxin molecules. A vermiculite sample tested in this research was ineffective as a mycotoxin adsorbent, presumably due to limited expansion.

Laser-diffraction particle-size analysis

Particle-size distribution by LDPSA was chosen to provide continuous histograms of the particle size efficiently in contrast to the size classes obtained by centrifuge methods. The particle-size distribution depends on the sample-dispersion treatment. This observation was used to develop Figure 6 where the particle size of the bulk sample in water *vs*. sodium hexametaphosphate (Na-hmp) solution and ultrasonic agitation can be compared. Thus, values on the *x* axis give an indication of the dispersability of the samples by two dispersion procedures. Combined chemical dispersion in the Na-hmp solution and physical ultrasound dispersion were selected to measure the abundance of colloidal particles available to adsorb AfB_1. Seven of the sets of curves indicate distinctly more dispersion where Na-hmp and ultrasound were employed (Figure 6). The Wyoming bentonite has a high pH and Na saturation and was dispersed even in water as expected (Table 2).

The three poorest adsorbents, 7AZ, 5OK, and 16MX, have a maximum volume percent (mode) above 5 μm and three of the four best adsorbents have mode values of <5 μm, suggesting that the coarser particles are less effective adsorbents of the mycotoxin molecules. The particles between 1 and 0.1 μm apparently contributed to the mycotoxin binding because they are more evident in three of the best adsorbents and are more abundant in sample 1MS than in the 3rd and 4th ranked adsorbents (Figure 6).

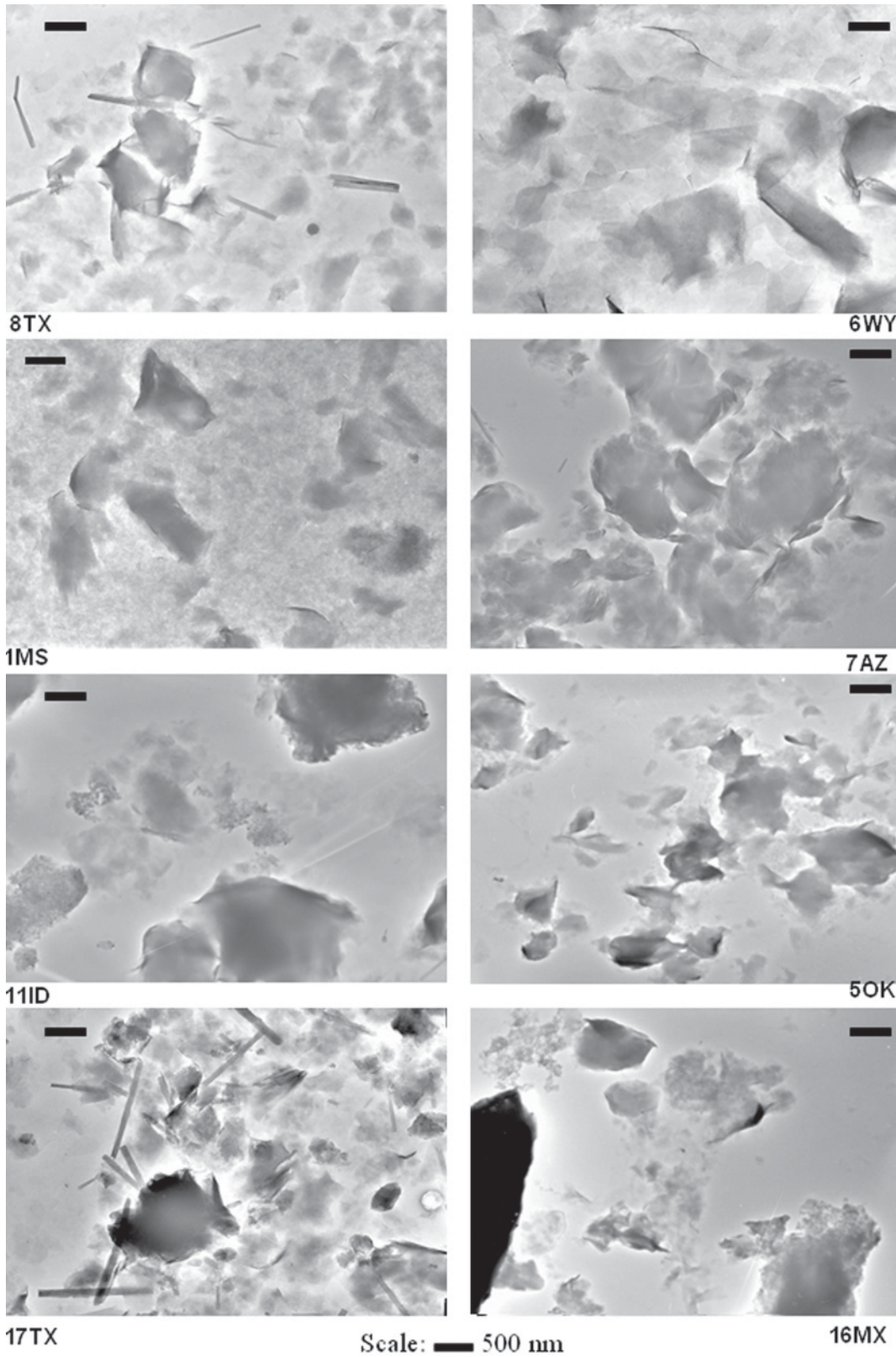

Figure 5. Electron micrographs of eight samples (scale bar = 500 nm). The better adsorbents are on the left and the poorer ones are on the right.

The particle size most indicative of reactive surfaces for binding AfB_1 is <2 μm, as indicated by the correlation of particle size and the mycotoxin adsorbed (Figure 7). Twelve adsorbent clays correlated (R^2 = 0.73) with the increase in dispersion in Na-hmp dispersive solution and the ultrasonic probe. Samples 6WY and LC1 did not follow the trend and were excluded from Figure 7. Both 6WY and LC1 behaved differently because they already

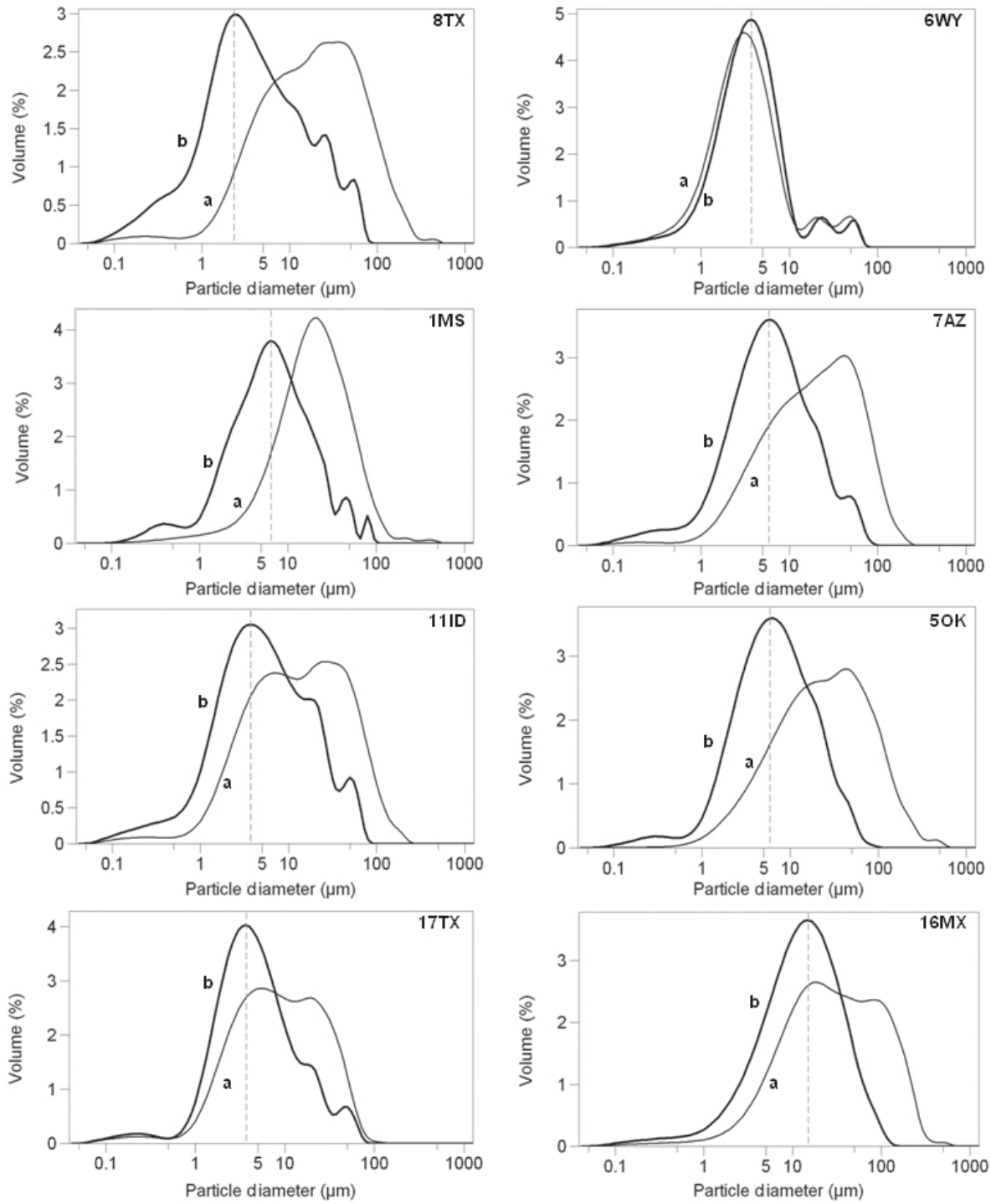

Figure 6. Histograms of particle-size distribution determined by laser diffraction analysis in distilled water (a) and Na-hexametaphosphate solution (b) with ultrasonic probe. Sample 6WY was only dispersed by shaking in water and Na-hexametaphosphate solution.

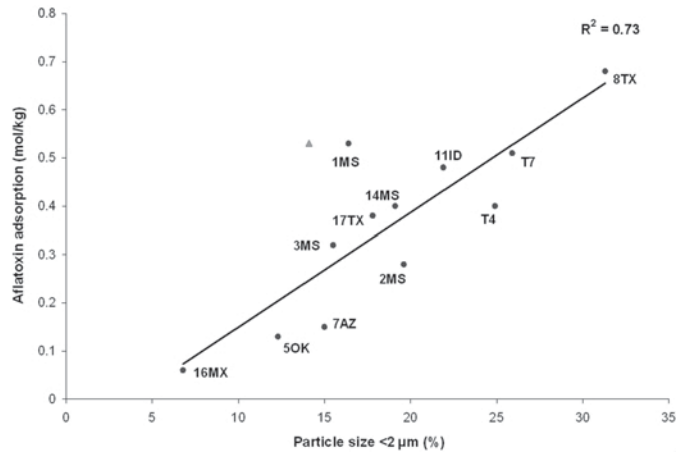

Figure 7. Aflatoxin adsorption *vs.* particle size by LDPSA (circular points). The triangular point represents the dispersion of sample 1MS without hand grinding.

dispersed in a high-Na environment and LC1 contained other minerals besides smectite, indicated by the low CEC.

DISCUSSION

The extent and conditions of AfB_1 adsorption have been modeled previously, and correlations evaluated with exchange cations and relationships with AfB_1 adsorption have been poor. In previous research, the adsorption of AfB_1 was between smectite layers (Kannewischer *et al.*, 2006). Recently, FTIR data showed that the octahedral composition of the smectites is an indicator of smectite quality as an AfB_1 adsorbent (Tenorio Arvide *et al.*, 2008). In this study properties that might influence the sequestration of AfB_1 were explored.

Fractionation in sodium carbonate solution

The loss of sample material during the fractionation procedure can be partially attributed to removal of carbonate as indicated by XRD data of whole materials in all samples that exhibited calcite peaks (Jackson, 2005). Sample 8TX exhibited dolomite peaks in XRD of the sand fraction even after the pre-treatment, which gave an indication of the presence of carbonates for that sample. The relatively large portion of the sand (Table 3) can mostly be explained by the presence of coarse, well crystallized minerals indicated by the narrow XRD peaks and by a small amount of un-dispersed, sand-sized smectite aggregates in sample 8TX. The silt fractions contain prismatic minerals and un-dispersed smectite. The silt-sized smectite is most evident in sample 11ID. Thus, the sodium carbonate dispersion procedure was not effective at completely removing smectite from the silt and sand fractions.

The large percentage of silt in sample 1MS is evident in the separated fractions (Table 3) and in the LDPSA curves (Figure 6), yet the sample performed well as an adsorbent of AfB_1 (discussed further below). Such persistent aggregates of smectite are consistent with bentonite genesis by the gradual dissolution of volcanic ash (glass, *etc*.) and the formation of complex particle morphology visible in the micrographs of Figure 4 for other samples (17TX, 5OK, and 16MX), suggesting the need for morphological characterization of bentonite silt fractions.

The fractionation procedure included steps to remove binding agents from the samples so the clay fractions could be dispersed more easily. Sodium saturation and drying of the smectites during the fractionation treatments reduced the sorption capacities of fractions as shown by their lower adsorption capacities for AfB_1 compared to the bulk, untreated samples (Table 1). Probable causes of lower AfB_1 adsorption by the fractions were a decrease in layer stacking order after Na dispersion and aggregation on oven drying (White, 1977). Differences in interlayer cation might also have contributed to reduction in adsorption behavior because Na is not as prone to hydrate as Ca. The Ca ions were the dominant exchange ion in the as-received smectite samples (Table 2). An implication of projecting these observations onto the intended application of smectites as AfB_1 adsorbents in animal diets is that excessive heating of smectite clay may influence their sorption capacity and thus should be avoided.

Table 3. Results of gravimetric fractionation.

Fraction	Sample			
	8TX	1MS	11ID	5OK
	Normalized wt.%			
Sand	3.6	18.6	2.4	13
Silt	13.7	40.5	18.8	16.3
Coarse clay	38.7	27.8	47.2	40.2
Fine clay	44	13.1	31.6	20.4

Langmuir Q_{max} values for the effective sorbent samples 8TX, 1MS, and 11ID were slightly (11ID) to very much (8TX) greater in the coarse-clay than in the fine-clay fractions (Table 1). This observation seems to indicate that the order and extent of stacking of the smectites is of importance to the adsorption process and also emphasizes that the main adsorption depends upon the accessibility of intact interlayers. According to these implications, edge sites and outer-surface sites, which are more abundant in the fine-clay fraction, might play a less important role in AfB_1 adsorption. Also, the isotherms of the clay fractions (Figure 2) have a linear shape and have a better fit to a straight line than to the Langmuir equation, *i.e.* C type (McBride, 1994). Essington (2004) described this adsorption behavior of linear partitioning as common for non-polar or hydrophobic organic compounds, indicating that the Freundlich model may be more appropriate. Nonetheless, the Langmuir function was useful to obtain comparative values for maximum adsorption.

Other minerals as adsorbents of aflatoxin

Palygorskite is a Si- and Mg-rich fibrous clay mineral with low CEC and large internal surface area, which has been reported to adsorb non-polar organic compounds (Singer, 2002). Palygorskite is known, in general, as a useful adsorbent for different purposes (*e.g.* decolorizing agent, animal bedding; Grim, 1962), yet was ineffective at AfB_1 adsorption. Assuming that for AfB_1 adsorption, the interlayer region is of pivotal importance, a small degree of adsorption by the palygorskite structure might be expected, since it does not possess continuous interlayers but instead has rectangular channels between opposing 2:1 ribbons joined by corner oxygens.

The structures of vermiculite and smectites resemble each other closely, and they have the same type of edge and outer-surface sites. The main difference lies in the greater layer charge of vermiculites, 0.6−0.9 per $O_{10}(0H)_2$, which is balanced by hydrated exchangeable cations (Malla, 2002). Adsorption of AfB_1 is assumed to be inhibited by the greater layer charge of vermiculite and restricted expansion compared to smectite. This gives another hint that the interlayer region is of pivotal importance to the adsorption of AfB_1. The illitic characteristics of components of the CC and FC fraction of sample 11ID (Figure 3e−f) indicate that the greater layer charge associated with illite compared to smectite might have reduced the adsorption ability of that sample by steric hindrance due to less opening of interlayer spaces compared to the overall, more smectitic samples, 8TX and 1MS. Also, the larger population of exchange cations in vermiculite and their associated water molecules may compete for space with the mycotoxin molecules that have relatively weak residual charge. Layer charge seems to be one of the mineralogical factors influencing adsorption and was a factor in the adsorption of the divalent organic cation, Diquat, which was adsorbed more in smectite than vermiculite (Dixon *et al.*, 1970).

Contrary to these findings, indicating the predominance of interlayer adsorption over edge-site and outer-surface adsorption, Phillips (1999) suggested multiple sites for reaction based on studies using Langmuir, Freundlich, Toth, and modified equations.

The differing mineralogy of the associated minerals in the samples, as indicated by XRD patterns (Figure 1) of their sand and silt fractions, indicate that these smectites were formed under different environmental conditions. They can form in soils as weathering crusts, in oceans, and through hydrothermal activity (Galán, 2006). Most commercial bentonites form mainly by alteration of volcanic ash deposits (Senkayi *et al.*, 1985) or authigenically in alkaline continental basins (Grim and Güven, 1978; Borchardt, 1989; Galán, 2006). The presence of dolomite in sample 8TX as well as calcite suggests formation from volcanic ash in shallow-marine environments, which is common for bentonites.

One hypothesis of this study was that, with the pure smectite phases in CC and FC fractions, the sorption potentials for AfB_1 should be similar for all samples, since no other phases dilute the adsorbent material. The adsorption isotherms for each fraction showed that this assumption was not justified and suggest that the differences in smectite properties, and not the properties of mineral phases that dilute the smectite, can influence their relative AfB_1 adsorption capacities.

Electron-optical examination of the samples provided information on sample structural properties and an indication of sample evolution. In the fractionated samples, detailed morphological features of individual smectites could be examined (Figure 3), while generic information in the unfractionated sample was often suggested by associated particles, such as glassy material, diatoms, and laths (Figure 4). The clay fractions of samples 8TX and 1MS both showed particles which were frequently folded (Figure 3a−d), as well as rather diffuse particles, which were common in all four samples. The clay fractions of sample 11ID contained well crystallized, illitic material, as indicated by the spot EDS pattern and the presence of a small amount of K.

The amount of very thin, cloud-like smectite particles decreases with decreasing AfB_1 sorption capacity (Figure 5; 8TX > 11ID > 17TX > 7AZ > 5OK > 16MX). The modal frequency of three of the best four sorbents is near 2 μm on the histogram (Figure 6). In contrast, for the three least effective sorbents in the right column, the modal frequency is >5 μm. An increased particle size thus determined would suggest that the smectite layers would become less accessible to the AfB_1 molecules which enter the interlayer spaces. From the particle-size histograms in Figure 6 we can, in general, conclude that the phosphate dispersant and ultrasonic agitation increased the dispersion, with the

obvious exception of Na-saturated sample 6WY, which is naturally well dispersed because of its greater Na saturation and high pH (Table 2).

The relationship of AfB_1 adsorption to the clay size fraction shows sample 1MS farther from the correlation line than the other data points (Figure 7). That observation prompted a supplemental experiment of manually grinding a small sample of 1MS bentonite for 15 min in a mortar under Na-hmp solution and periodically checking particle size with the laser instrument after 1 min of ultrasonic dispersion. The LDPSA indicated an increase in clay content and the plot was modified as shown in Figure 7 and the correlation was improved from 66% to 73%. The first-order XRD basal spacing was strengthened and the prismatic 020 was much reduced by supplemental grinding of the sample. It is interesting to note that the aggregation in the initial bentonite did not drastically reduce the amount of AfB_1 adsorbed. Similarly, a bentonite from Spain had a high CEC yet it did not have colloidal properties and was found, by scanning electron microscopy, to contain abundant silt-size aggregates (Reid-Soukup and Ulery, 2002).

Applications

The minerals (quartz, feldspar, and dolomite) associated with smectite in bentonite are coarse and relatively stable phases that are unlikely to have a negative chemical influence on the diet of animals. The excess sand in two of the four bentonites fractionated may not bode well for their use as adsorbents due to dilution of the smectite and unfavorable physical properties during processing. The presence of gypsum laths in two of the bentonites is unlikely to have adverse dietary influence since it is relatively soluble and calcium sulfate is an ingredient in some human foods. The use of the LDPSA and FTIR are time-saving instruments that will improve bentonite evaluation efficiency.

CONCLUSIONS

Good adsorbents of AfB_1 can be identified using LDPSA by obtaining the particle-size distribution with Na-hmp solution as the dispersion medium and mechanical agitation using an ultrasonic probe. Oven drying of the smectite degraded its adsorption capacity, presumably because of changes in porosity and particle size. Particle size gives the best correlation for AfB_1 adsorption but it does not, by itself, explain the total effectiveness of the smectite clays. Additional properties, including the porosity of the silt fraction from different bentonites, have to be evaluated to better understand the adsorption mechanism and variability in clay composition as shown in a parallel study (Tenorio Arvide *et al*., 2008).

The TEM images show many typical thin sheets with folds and curves as well as thicker smectite particles. Also, they show three-dimensional phases suggestive of opal or prismatic minerals in complex shapes.

Vermiculite and palygorskite, which are used as adsorbents for other purposes, were poor adsorbents of AfB_1.

ACKNOWLEDGMENTS

Special thanks to Editors Joe Stucki and Kevin Murphy, and to the anonymous reviewers for their helpful comments.

REFERENCES

Borchardt, G. (1989) Smectites. Pp. 675–728 in: *Minerals in Soil Environments* (J. B. Dixon and S. B.Weed, editors). Soil Science Society of America, Madison, Wisconsin.

Desheng, Q., Fan, L., Yanhu, Y., and Niya, Z. (2005) Adsorption of aflatoxin B1 on montmorillonite. *Poultry Science*, **84**, 959–961.

Dixon, J.B., Moore, D.E., Agnihotri, N.P., and Lewis, D.E. (1970) Exchange of Diquat (2+) in soil clays, vermiculite, and smectite. *Soil Science Society of America Proceedings*, **34**, 805–808.

Dixon, J.B., Kannewischer, I., Tenorio Arvide, M.G. and Barrientos Velásquez, A.L. (2008) Aflatoxin sequestration in animal feeds by quality-labeled smectite clays: An introductory plan. *Applied Clay Science*, **40**, 201–208.

Essington, M.E. (2004) *Soil and Water Chemistry – An Integrative Approach.* CRC Press, Boca Raton, Florida, USA.

Galán, E. (2006) Genesis of clay minerals. Pp. 1129–1162 in: *Handbook of Clay Science* (F. Bergaya *et al.*, editors). Elsevier, Amsterdam.

Grim, R.E. (1962) *Applied Clay Mineralogy*. McGraw-Hill Book Company Inc., New York.

Grim, R.E. and Güven, N. (1978) *Bentonites: Geology, Mineralogy, Properties and Uses*. Developments in Sedimentology, Elsevier, Amsterdam.

Holzenburg, A., Flint, T.D., Shepherd, F.H., and Ford, R.C. (1996) Photosystem II: Mapping the location of the oxygen evolution-enhancing subunits by electron microscopy. *Micron*, **27**, 121–127.

Jackson, M.L. (2005) *Soil Chemical Analysis – Advanced Course*. 2nd edition. Parallel Press, University of Wisconsin, Madison Libraries, Madison, Wisconsin, USA.

Kannewischer, I., Tenorio Arvide, M.G., White, G.N., and Dixon, J.B. (2006) Smectite clays as adsorbents of Aflatoxin B1: Initial Steps. *Clay Science, Japan*, **12,** Supplement 2, 199–204.

Kunze, G.W. and Dixon, J.B. (1986) Pretreatment for mineralogical analysis. Pp. 91–100 in: *Methods of Soil Analysis, Part 1. Physical and Mineralogical Methods*. Agronomy Monograph no. **9**, American Society of Agronomy-Soil Science Society of America, Madison, Wisconsin.

Lee, K.-M., Herrman, T.J., Langenfelser, J., and Jackson, D.S. (2005) Classification and prediction of maize hardness-associated properties using multivariate statistical analyses. *Journal of Cereal Science*, **41**, 85–93.

Malla, P.B. (2002) Vermiculites. Pp. 501–530 in: *Soil Mineralogy with Environmental Applications* (J.B. Dixon and D.G. Schulze, editors). Book series no. **7**, Soil Science Society of America, Madison, Wisconsin.

Mering, J. and Oberlin, A. (1967) Electron-optical study of smectites. *Clays and Clay Minerals*, **15**, 3–25.

Pavão, A.C., Neto, L.A.S., Neto, J.F., and Leão, M.B.C. (1995) Structure and activity of aflatoxins B and G. *Journal of*

Molecular Structure: THEOCHEM, **337**, 57–60.
Phillips, T.D. (1999) Dietary clay in the chemoprevention of aflatoxin-induced disease. *Toxicological Sciences* **52** (Supplement), 118–126.
Phillips, T.D., Sarr, A.B., and Grant, P.G. (1995) Selective chemisorption and detoxification of alflatoxins by phyllosilicate clay. *Natural Toxins*, **3**, 204–213.
Phillips, T.D., Lemke, S.L., and Grant, P.G. (2002) Characterization of clay-based enterosorbents for the prevention of aflatoxicosis. *Advances in Experimental Medicine and Biology*, **504**, 157–171.
Reid-Soukup, D.A. and Ulery, A.L. (2002) Smectites. Pp. 467–500 in: *Soil Mineralogy with Environmental Applications* (J.B. Dixon and D.G. Schulze, editors). Soil Science Society of America, Madison, Wisconsin.
Sarr, A.B., Clement, B.A., and Phillips, T.D. (1991) Molecular mechanism of aflatoxin B1 chemisorption by hydrated sodium calcium aluminosilicate (abstract). *Toxicologist*, **7**, 97.
Senkayi, A.L., Dixon, J.B., Hossner, L.R., and Kippenberger, L.A. (1985) Layer charge evaluation of expandable soil clays by an alkylammonium method. *Soil Science Society of America Journal*, **49**, 1054–1060.
Singer, A. (2002) Palygorskite and sepiolite. Pp. 555–583 in: *Soil Mineralogy with Environmental Applications* (J.B. Dixon and D.G. Schulze, editors). Book series no. **7**, Soil Science Society of America, Madison, Wisconsin.
Tenorio Arvide, M.G., Mulder, I., Barrientos Velazquez, A.L., and Dixon, J.B. (2008) Smectite clay adsorption of aflatoxin versus octahedral composition, as indicated by FTIR. *Clays and Clay Minerals*, **56**, 571–578.
Urbanek, R. (1997) Syntheses and Mechanistic Studies of the Potent Mycotoxin Aflatoxin B_1. Student seminar program for organic and biological specialty areas. Department of Chemistry, University of Minnesota, USA.
White, J.L (1977) Preparations of specimens for infrared analysis. Pp. 847–863 in: *Minerals in Soil Environments* (J.B. Dixon and S.B. Weed, editors). Soil Science Society of America, Madison, Wisconsin, USA.
White, G.N. and Dixon, J.B. (2003) *Soil Mineralogy Laboratory Manual.* 9th edition. Published by the authors, Department of Soil and Crop Sciences. Texas A&M University, College Station, Texas 77843–2474, USA. http://soilcrop.tamu.edu/professors/dixon/profile.htm

(*Received 1 February 2007; revised 5 August 2008; A.E. P. Komadel*)